J. Korean Inst. Electr. Electron. Mater. Eng.
Vol. 38, No. 1, pp. 1-7 January 2025
doi: https://doi.org/10.4313/JKEM.2025.38.1.1
ISSN 1226-7945(Print), 2288-3258(Online)

Academic Progress Report

Localized Stress-Enhanced Piezoelectricity of Anisotropic Barium Titanate Nanowires in Piezoelectric Composites for Application in Healthcare Sensors

Yumin Kwon[1], Yubin Kim[1], Hoseok Lee[2], and Minjeong Ha[1]

[1] School of Materials Science and Engineering, Gwangju Institute of Science and Technology (GIST), Gwangju 61005, Korea

[2] Institute of Advanced Composite Materials, Korea Institute of Science and Technology (KIST), Wanju 55324, Korea

(Received November 4, 2024; Revised November 22, 2024; Accepted November 22, 2024)

Abstract: The search for sustainable and efficient energy conversion technologies is becoming increasingly critical in response to global energy and environmental challenges. Traditional lead-based piezoelectric materials, such as lead zirconate titanate (PZT), have high piezoelectric constant but present significant health problems and environmental risks due to their hazardous metal contaminants. This study addresses these concerns by investigating barium titanate (BTO), a lead-free alternative, and enhancing its performance using anisotropic nanowires (NWs) structures. BTO NWs were synthesized via a two-step hydrothermal method and incorporated into a poly(vinylidene fluoride-trifluoroethylene) [P(VDF-TrFE)] matrix to fabricate a piezoelectric composite film. The resulting device demonstrated a notable increase in electrical output compared to devices based on isotropic morphology of BTO nanoparticles, exhibiting enhanced performance. These findings suggest that BTO NWs hold significant promise for applications in flexible and wearable electronics, paving the way for further advancements in sustainable energy technology.

Keywords: Anisotropy, Barium titanate nanowire, Piezoelectricity, Self-powered sensor, Composite

1. INTRODUCTION

The depletion of fossil fuels and the resulting environmental degradation have significantly increased global interest in renewable energy sources such as solar, wind, hydroelectric, geothermal, and biomass energy [1-7]. While these energy sources can generate substantial power, they often face limitations due to temporal and spatial constraints, and the initial costs of establishing energy conversion infrastructure can be high [8,9]. Consequently, there is a growing need for compact, sustainable energy-harvesting solutions that can supply power to the electronic devices we use in daily life without frequent battery recharging. One promising approach is converting kinetic energy from human movement or ambient mechanical vibrations into electricity [10,11]. This method not only reduces dependence on battery but also enables the quantitative transduction of mechanical stimuli into electrical signals, making it suitable for applications of physical sensors such as axial force sensing, motion detection, and ambient vibration/acoustic wave sensing. A widely explored mechanism for such energy conversion is the piezoelectric effect, which arises from electromechanical interactions in non-centrosymmetric crystals [12].

Lead zirconate titanate (PZT) has long been a popular thin-film piezoelectric material due to its high dielectric and

✉ **Minjeong Ha; minjeongha@gist.ac.kr**

Yumin Kwon and Yubin Kim contributed to the work equally.

piezoelectric constants (d_{33}=225~590 pC/N) [13]. PZT is a ferroelectric material capable of maintaining spontaneous polarization, with its crystal structure featuring electric dipoles that are aligned in specific directions and readily reoriented under applied external forces [14]. However, the significant environmental and health risks associated with PZT, particularly due to the release of hazardous metal contaminants during sintering and processing, have intensified research efforts aimed at developing lead-free piezoelectric materials [15]. Among the lead-free alternatives, $BaTiO_3$ (BTO) has garnered attention as a promising candidate due to its high piezoelectric constant (d_{33}=191 pC/N) [16]. The superior piezoelectric performance of BTO is largely attributed to the Ti atom (Ti^{4+}) within the BTO lattice, which can possess significant potential due to its high charge and small atomic size [17]. However, despite its impressive piezoelectric characteristics, inherent brittleness of BTO poses challenges for developing human-interactive flexible devices including wearable gadgets, implantable medical devices, and health-monitoring systems [18].

To address this limitation, BTO particles have been embedded into polymers for enhancing flexibility and mechanical resilience in polydimethylsiloxane (PDMS), polyvinylidene fluoride (PVDF), poly(vinylidene fluoride-*co*-hexafluoropropylene) [P(VDF-HFP)], poly(vinylidene fluoride-trifluoroethylene) [P(VDF-TrFE)], and cellulose [19-22]. However, this approach presents challenges as the viscoelastic nature of the polymer matrix absorbs much of the external mechanical stress, limiting effective stress transfer to the BTO particles. Moreover, low dispersity and connectivity of BTO particles further reduce mechanical stress transmission, weakening the electromechanical response and polarization. For the strong percolation network and effective stress transmission between the inorganic fillers within the polymer matrix, diverse structural designs of anisotropic BTO have been investigated, including nanocubes (NC), nanowires (NW), and nanosheets (NS). Alluri et al. developed flexible and high piezoelectric output energy harvesting devices based on BTO NC embedded into PDMS [21]. The single-phase perovskite structure of BTO NC has been shown to offer superior piezoelectric and ferroelectric properties compared to the non-piezoelectric cubic phase. Wu et al. enhanced the piezocatalytic effect by utilizing BTO NW, as the piezoelectric potential of one-dimensional or two-dimensional piezoelectric materials is greater than that of nanoparticles (NP) due to their inherent ability to achieve higher potential through stress confinement [23]. Tang et al. studied BTO 2D NS to create a high performance piezocatalyst using its large surface area for receiving mechanical impact [24]. For high aspect ratio (AR) piezoelectric NW, the anisotropic structure enables mechanical stress confinement when longitudinal axis of NWs aligns with the direction of applied external stress. This stress confinement enhances the dipole moment and polarization induction [25]. Additionally, the high AR NWs enables to form an effective percolation network with a high probability of connecting to each other, resulting in effective mechanical-to-electrical energy conversion due to the stress transfer of 3D interconnected NWs [18].

In this study, we synthesized high AR BTO NW using a two-step hydrothermal method. This BTO NW demonstrated

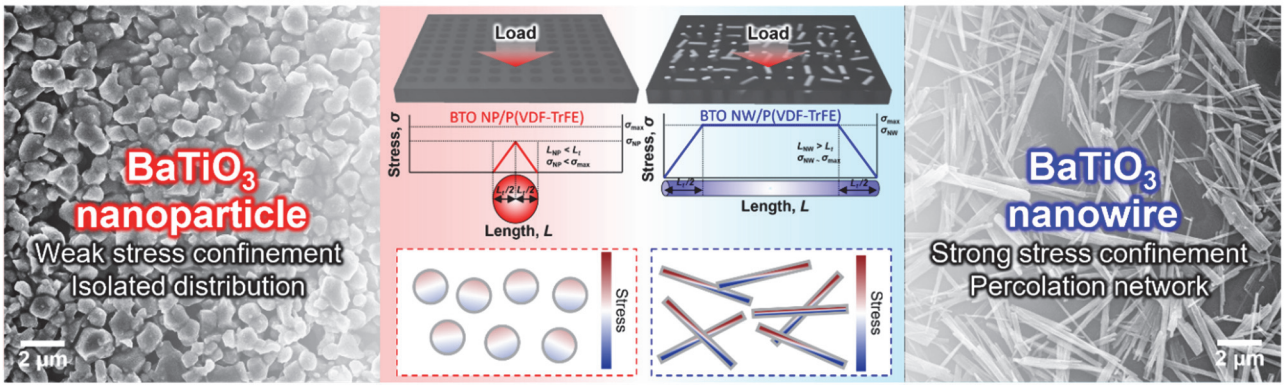

Fig. 1. Schematic overview of the conceptional design for localized stress-enhanced piezoelectricity of anisotropic BTO NW.

a high tetragonal phase ratio, which is critical for maximizing the piezoelectric constant. The tetragonal structure of BTO NW exhibits a net polarization along the [001] edge direction due to the displacement of the Ti^{4+} cation from the center of the TiO_6 octahedron, leading to a separation between the cation and anion centers that contributes to strong piezoelectric signals [26]. Furthermore, BTO NW was embedded in P(VDF-TrFE) as piezoelectric polymer composites, which exhibit high flexibility (bending radius: ~0.3 mm^{-1}). The resulting composites consisting of highly interconnected BTO NW exhibited a 1.58-fold increase in output voltage compared to those involving BTO NP under vertical pressure because of enhanced stress transmission and propagation. Our flexible piezoelectric sensors can be worn on the curved human skin and sensing minute wrist pulse for the application of daily healthcare devices.

2. EXPERIMENTAL SECTION

Barium titanate ($BaTiO_3$, 99.5%), titanium dioxide (TiO_2, 99.7%), and barium hydroxide octahydrate [$Ba(OH)_2{\cdot}8H_2O$, 98%] were purchased from Sigma-Aldrich. Sodium hydroxide (NaOH, 98.0%), and hydrochloric acid (HCl, 37%) were obtained from Tokyo Chemical Industry. Poly(vinylidene fluoride-*co*-trifluoroethylene) [P(VDF-TrFE), 70/30 copolymer] was provided from Piezotech. N,N-dimethylformamide (DMF, 99.5%) was purchased from Duksan Pure Chemicals.

BTO NW was synthesized through a two-step hydrothermal reaction. Initially, 1.5 g of TiO_2 was added to 60 mL of an aqueous solution of 10 M NaOH and magnetically stirred for 12 h. The mixture was then transferred into a 100 mL Teflon-lined stainless autoclave, which was heated at 180°C for 48 h. The resulting $Na_2Ti_3O_7$ NW was washed with deionized water by repeated centrifugation and redispersion. In the final cycle, $Na_2Ti_3O_7$ NW was soaked in an aqueous solution of 0.2 M HCl for 24 h to obtain $H_2Ti_3O_7$ NW. $H_2Ti_3O_7$ NW was neutralized with deionized water and dried at 65°C overnight under vacuum. In a second hydrothermal reaction, 0.14 g of $H_2Ti_3O_7$ and 1.025 g of $Ba(OH)_2{\cdot}8H_2O$ corresponding to 2 equivalent moles of Ti were dispersed in 60 mL of deionized water by ultrasonication. The suspension was transferred to a 100 mL Teflon-lined stainless autoclave and kept at 200°C for 1.5 h. Finally, the synthesized BTO NW was washed successively with an aqueous solution of 0.2 M HCl, deionized water, and ethanol, then dried at 65°C overnight under vacuum condition.

BTO/P(VDF-TrFE) composite films were fabricated through the solution casting technique. In brief, BTO NP and NW were dispersed into 10 wt% DMF solutions of P(VDF-TrFE) using Planetary High Velocity Mixer (400-DI, Hanil Global Technology). The mixtures were cast onto glass Petri dishes and dried at 120°C for 4 h under vacuum condition. In this step, the thickness of composite films could be adjusted by pipetting different volumes of the mixture solutions. The thickness of composite films was ~100 μm throughout this study unless otherwise specified. The resulting films were finally cut into the size of 2×4 cm^2.

Field-emission scanning electron microscopy (FE-SEM) images were obtained using JSM-7,500F (JEOL Ltd.). For FE-SEM images of the nanomaterials, an aliquot of aqueous suspensions of NPs or NWs was dropped onto Si wafer. To record X-ray diffraction (XRD) patterns of BTO, the identical aqueous suspensions of BTO were dropped onto a glass slide, and the deposited particles were scanned in a range from 20° to 80° utilizing D/MAX-2500 (Rigaku). The electric output performance of the piezoelectric composite films was examined upon repeated compression/release cycles. For this purpose, the composite films sandwiched with Cu electrodes were placed on a linear motor (JIPT, JUNIL TECH) and external wires were further extended to a digital multimeter (DMM7510, Keithley). A vertical load with a frequency of 0.5 Hz was periodically applied to the piezoelectric composite films to record an electric response. Note, the magnitude of generated voltage signals was averaged from three identical films prepared independently. The compressive load was monitored with a digital force gauge (AI-35T, CASKOREA) and the level of pressure was separately calculated afterward.

3. RESULTS AND DISCUSSION

To synthesize BTO NW with a high AR, a two-step hydrothermal method utilizing an alkali metal nano-template was approached as depicted in the sequential schematics [Fig. 2(a)]. At the first step, a sodium-centered NW as the nano-template ($Na_2Ti_3O_7$) was hydrothermally synthesized with TiO_2 particle and an aqueous solution of NaOH [Fig. 2(c)]. Under a strong basic condition, the infiltration of Na^+ ion into

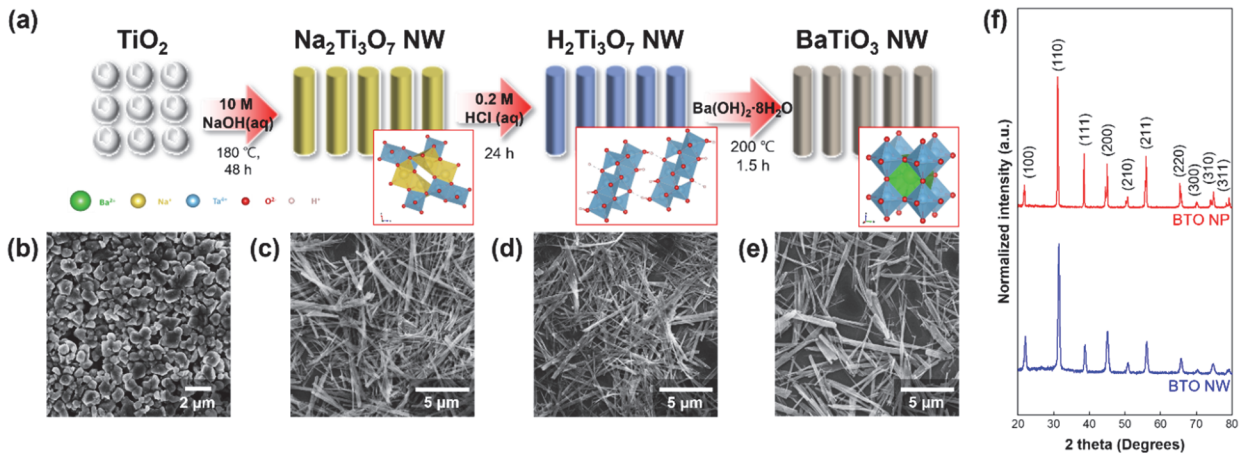

Fig. 2. (a) Sequential schematics of the synthesis of BTO NW. FE-SEM images of (b) BTO NP, (c) $Na_2Ti_3O_7$ NW, (d) $H_2Ti_3O_7$ NW, (e) BTO NW, and (f) XRD patterns corresponding to BTO NP (red line) and BTO NW (blue line).

a layered TiO_2 particle is favorably facilitated by stabilizing an interlayer space reported as Ostwald rule. In this step, the TiO_2 particle undergoes dissolution and re-assembly into an aligned TiO_6 octahedron, leading to further crystallographic transition to form one-dimension-directed crystal with an elongated morphology [27]. Next, $Na_2Ti_3O_7$ NW was further converted to $H_2Ti_3O_7$ NW through an acid treatment [Fig. 2(d)], which offers an open-structured lattice through an ion-exchange reaction [28]. In the second hydrothermal reaction, because the open crystal structure provides a more favorable site for a following exchange reaction with Ba^{2+} ion dissociated from $Ba(OH)_2{\cdot}8H_2O$, Ba^{2+} ion readily replaces the crystallographic vacancy of $H_2Ti_3O_7$ NW, resulting in the production of BTO NW [Fig. 2(e)].

In Figs. 2(b)~(e), SEM images of commercially available BTO NP and the synthesized NW are represented. The resulting BTO NW exhibited a higher AR of ~11.4 with an approximate length of ~1.9 μm and a diameter of ~0.17 μm, compared to the relative isotropic morphology of BTO NP with a diameter of ~0.74 μm. In addition, XRD spectra of BTO NW reveal no noticeable peaks corresponding to undesirable by-products (e.g. $BaCO_3$) expected to emerge during the reaction and a similar pattern to that of tetragonal BTO NP [Fig. 2(f)], which proves the successful synthesis of BTO NW.

To investigate the effectiveness of the anisotropic structure of BTO NWs in facilitating the formation of a percolation network, BTO NP and BTO NW were incorporated into P(VDF-TrFE) which has the benefits of mechanical resilience, ease of processing, and synergetic effect on improving electric output based on the piezoelectric nature of P(VDF-TrFE). First, BTO NP and BTO NW powders were dispersed into separate DMF solutions of P(VDF-TrFE) and then the mixtures were cast to obtain homogeneous composite films (see more detailed procedures in Experimental section). To study different geometrical effects of the piezoelectric nanofillers on an electric response signal, a desirable amount of BTO nanofillers between the corresponding percolation thresholds of BTO NP and NW was loaded to the composites [$\Phi_{c\ BTO\ NW}$=0.370 wt%, $\Phi_{c\ BTO\ NP}$=4.214 wt% based on a theoretical expectation in Fig. 3(c-i)] [29]. To fabricate a piezoelectric sensor, the resulting films were sandwiched with Cu foils as an electrode material and poled under an electric field (20 kV mm^{-1}). Concurrently, the Cu foils were conformally glued to a non-conductive glass slide to prevent any triboelectric contributions during measurements, as triboelectricity arises when different materials come into frictional contact and generates unwanted charges that create noise. This ensures that only the inherent electrical properties of the Cu foils are measured, minimizing interference from external charge generation [Fig. 3(a)]. A typical piezoelectric signal of the as-fabricated sensing devices under a vertical pressure is shown in Fig. 3(c-ii). The sensors generated AC voltage profiles increasing towards positive under compression, and decreasing towards negative under releasing, resulting from the internal polarization of electric dipoles [Fig. 3(b)]. For a more quantitative study of the geometric effect of BTOs on a response signal, open-circuit voltage of the neat P(VDF-TrFE)

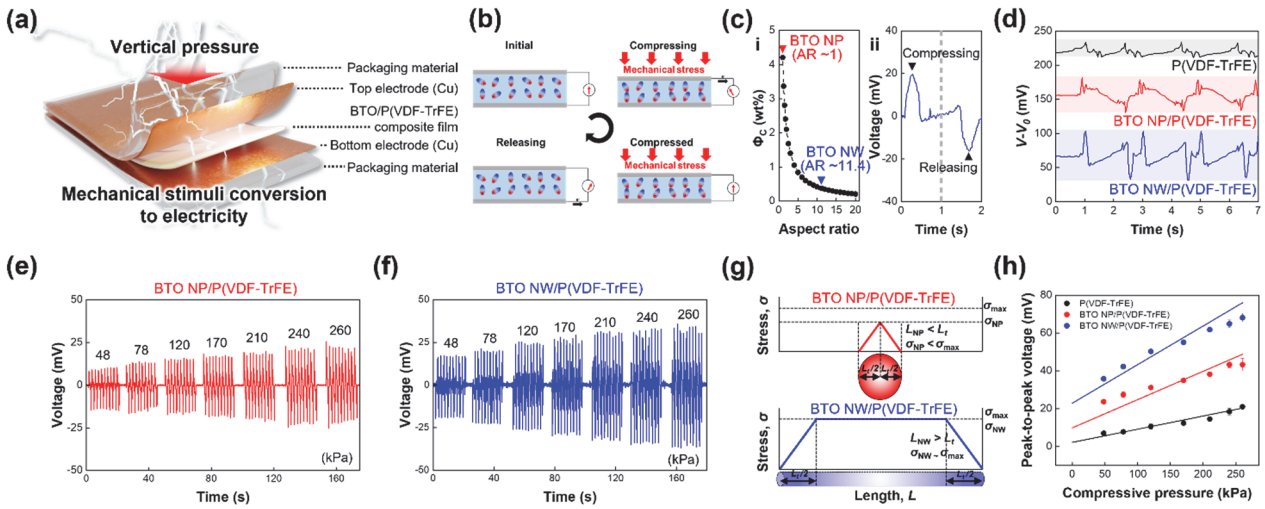

Fig. 3. Schematic illustration of (a) the configuration of the piezoelectric sensor and (b) mechanical pressure to electricity conversion mechanisms. (c-i) Theoretical expectation of percolation threshold for nanofillers with different aspect ratio. Open-circuit voltage profile for (c-ii) the piezoelectric sensor under an external compression/release cycle and (d) P(VDF-TrFE) (highlighted in a black box), BTO NP/P(VDF-TrFE) (red box), and BTO NW/P(VDF-TrFE) (blue box) sensors upon repeated compression/release cycles. Vertical pressure induced voltage signals of (e) BTO NP/P(VDF-TrFE) and (f) BTO NW/P(VDF-TrFE) recorded with a pressure range from 48 kPa to 260 kPa, (g) simplified schematic representation of stress distribution profiles for simplified piezoelectric nanofillers under pressure, and (h) sensitivity plots of P(VDF-TrFE) (black), BTO NP/P(VDF-TrFE) (red), and BTO NW/P(VDF-TrFE) (blue) sensors with respect to the magnitude of pressure applied.

and the composite sensors was compared in Fig. 3(c). When a compressive pressure was periodically repeated compression/release cycles at 260 kPa, BTO NP/P(VDF-TrFE) and BTO NW/P(VDF-TrFE) composite sensors generated a peak-to-peak voltage of ~43 mV (denoted as a red line) and ~68 mV (blue line) respectively, which were more sensitively responsive compared to the output voltage of neat P(VDF-TrFE) sensor (~20 mV, black line). This is ascribed to the incorporation of the piezoelectric nanofillers with a high piezoelectric constant into the matrix with relatively lower constant ($d_{33\ BTO}$=191 pC N^{-1}, $d_{33\ P(VDF\text{-}TrFE)}$=19.8 pC N^{-1}) [30], hence improving the magnitude of polarization generated even under the same level of applied mechanical pressure. One should note that when the magnitude of pressure applied to the sensors was gradually increased with a range from 48 kPa to 260 kPa, the magnitude of voltage generated from BTO NW/P(VDF-TrFE) sensor was more rapidly increased with respect to the applied pressure (0.158 mV kPa^{-1}) than that of BTO NP/P(VDF-TrFE) (0.091 mV kPa^{-1}) [Fig. 3(e) and (f)]. Based on load transfer theory, external compressive load exerted to a polymer composite system initially propagates across a matrix. Then, it encounters an interface with a nanofiller randomly distributed in the matrix, and finally transfers to the nanofiller. At this stage, the compressive stress would be focused at the nanofiller in that piezoelectric ceramics typically possess relatively higher mechanical stiffness than polymeric matrix. Because of the presence of load transfer zone (L_t) across the direction of which a load is delivered, the level of load transfer and stress confinement on the nanofiller significantly depends on inherent AR of a nanofiller geometry [31] (see the schematic representation in Fig. 3(g)). Consequently, less stress is concentrated in an isotropic BTO NP, resulting in lower polarization compared to a BTO NW, which can be observed in the difference of sensitivities between BTO NP/P(VDF-TrFE) and BTO NW/P(VDF-TrFE) composites (Fig. 3(h)). Futhermore, with modeled loading concentration of piezoelectric nanofillers (1 wt%) that lies between the percolation thresholds for BTO NP and NW, anisotropic NWs achieve a percolated configuration, whereas BTO NP tends to remain more isolated within the matrix. This configuration allows local fields generated by individual NWs under mechanical stress to synergistically enhance one another, resulting in the higher sensitivity observed in BTO NW/P(VDF-TrFE) composites.

As a proof-of-concept experiment, BTO NW/P(VDF-TrFE)

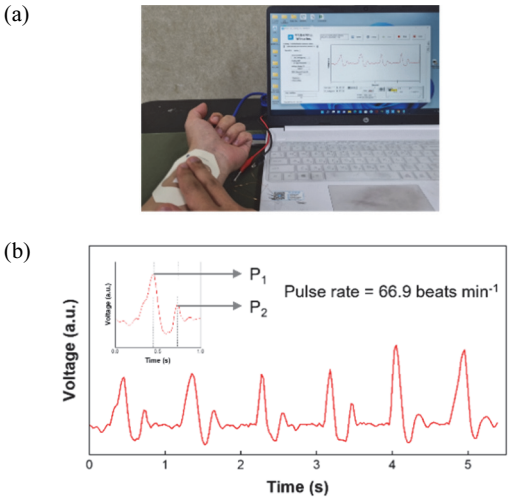

Fig. 4. (a) Heartbeat pulse monitoring experiment and (b) the corresponding acquisition of response signals.

sensor was attached onto a wrist as a healthcare sensor device to monitor heartbeat pulse, which is one of the important biophysical signals for the diagnosis of cardiovascular diseases. To avoid delamination from human skin, a thin adhesive patch (3M Tegaderm, 6×7×0.015 cm^3) was further applied onto BTO NW/P(VDF-TrFE) sensor [Fig. 4(a)]. As shown in Fig. 4(b), two characteristic peaks in a periodically repeated response signal were identified, which corresponds to P_1 and P_2 between the systolic and diastolic pulse at a radial artery of a volunteer [32]. These results represent an average heartbeat rate is ~67 beats min^{-1}, highlighting the potential use of BTO NW/P(VDF-TrFE) in a daily health monitoring device. Also, using our device, we were able to determine the wrist artery augmentation index (P_2/P_1), which correspond to P_1 is the (voltage value of P_1 peak - baseline voltage value), and P_2 is the (voltage value of P_2 peak - baseline voltage value). For a healthy male in 20's, the average index typically falls within the range of 0.4 to 0.6. The participant in our study, who was also a healthy male in 20's, exhibited an appropriate value of 0.457±0.096, confirming the reliability of our measurement system [33].

4. CONCLUSION

In conclusion, the enhanced piezoelectric performance observed in BTO NWs compared to BTO NPs is attributed from several critical factors, including efficient stress confinement and the formation of a robust percolation network. The anisotropic structure of BTO NWs effectively confines stress, enhancing dipole alignment and polarization under mechanical stress, which in turn improves piezoelectric potential generation. Moreover, the high AR of NWs facilitates the formation of a 3D interconnected percolation network within polymer composite films, allowing for effective stress transmission and propagation throughout the matrix, thereby maximizing overall piezoelectric output. Unlike Pb-based materials such as PZT, lead magnesium niobate-lead titanate (PMN-PT), and lead lanthanum zirconate titanate (PLZT), BTO is free from health and environmental concerns during processing. Despite such merits, BTO inherently possesses a lower piezoelectric constant compared to Pb-based materials, resulting in relatively low output to the piezoelectric composites. Even in the situation where BTO NWs are embedded in viscous polymer matrix, the amount of net potential generation will be degraded. This limitation can be addressed by improving the dispersion and alignment of the BTO NWs in the polymer matrix. The dispersion of BTO NWs within the polymer matrix can be achieved by a dispersant with strong chelating ability. In addition, long-range alignment of BTO NWs matched with the direction of applied stress can effectively transit the mechanical energy into electricity. Based these approaches, BTO NWs could achieve enhanced piezoelectric output with high signal-to-noise level while maintaining their lead-free and biocompatible properties, making them suitable for applications in body-implanting device, biomedical engineering, wearable health monitoring system, and IoTs with energy harvesting solutions.

ORCID

Minjeong Ha https://orcid.org/0000-0002-6635-7462

ACKNOWLEDGEMENT

This work was supported by the National Research Foundation of Korea (NRF) grant funded by the Korea government (MSIT) (No.RS-2023-00207836, 2022R1C1C1004845).

REFERENCES

[1] S. Bakhsh, W. Zhang, K. Ali, and J. Oláh, *Energy Strategy Rev.*, **52**, 101330 (2024).
doi: https://doi.org/10.1016/j.esr.2024.101330

[2] E. Barbier, *Renewable Sustainable Energy Rev.*, **6**, 3 (2002).
doi: https://doi.org/10.1016/S1364-0321(02)00002-3

[3] N. Kannan and D. Vakeesan, *Renewable Sustainable Energy Rev.*, **62**, 1092 (2016).
doi: https://doi.org/10.1016/j.rser.2016.05.022

[4] A. I. Osman, L. Chen, M. Yang, G. Msigwa, M. Farghali, S. Fawzy, D. W. Rooney, and P. S. Yap, *Environ. Chem. Lett.*, **21**, 741 (2023).
doi: https://doi.org/10.1007/s10311-022-01532-8

[5] B. Shi, Q. Wang, H. Su, J. Li, B. Xie, P. Wang, J. Qiu, C. Wu, Y. Zhang, X. Zhou, and T. W. Kim, *Nano Energy*, **116**, 108789 (2023).
doi: https://doi.org/10.1016/j.nanoen.2023.108789

[6] C. Wang, S. A. Raza, T. S. Adebayo, S. Yi, and M. I. Shah, *Energy*, **262**, 125303 (2023).
doi: https://doi.org/10.1016/j.energy.2022.125303

[7] D. Zhou and Z. Deng, *Renewable Sustainable Energy Rev.*, **78**, 23 (2017).
doi: https://doi.org/10.1016/j.rser.2017.04.086

[8] Q. Hassan, S. Algburi, A. Z. Sameen, H. M. Salman, and M. Jaszczur, *Results Eng.*, **20**, 101621 (2023).
doi: https://doi.org/10.1016/j.rineng.2023.101621

[9] G. E. Halkos and E. C. Gkampoura, *Energies*, **13**, 2906 (2020).
doi: https://doi.org/10.3390/en13112906

[10] S. Bai, J. Cui, Y. Zheng, G. Li, T. Liu, Y. Liu, C. Hao, and C. Xue, *Appl. Energy*, **329**, 120292 (2023).
doi: https://doi.org/10.1016/j.apenergy.2022.120292

[11] J. Xu, T. Tat, X. Zhao, X. Xiao, Y. Zhou, J. Yin, K. Chen, and J. Chen, *ACS Nano*, **17**, 3865 (2023).
doi: https://doi.org/10.1021/acsnano.2c12142

[12] W. Chen, Q. Zheng, Y. A. Lv, Y. Chen, Q. Fan, X. Zhou, H. Li, Q. Yu, and H. Liu, *Chem. Eng. J.*, **465**, 142755 (2023).
doi: https://doi.org/10.1016/j.cej.2023.142755

[13] X. Chen, S. Xu, N. Yao, W. Xu, and Y. Shi, *Appl. Phys. Lett.*, **94**, 253113 (2009).
doi: https://doi.org/10.1063/1.3157837

[14] E. Venkatragavaraj, B. Satish, P. R. Vinod, and M. S. Vijaya, *J. Phys. D: Appl. Phys.*, **34**, 487 (2001).
doi: https://doi.org/10.1088/0022-3727/34/4/308

[15] T. Ibn-Mohammed, I. M. Reaney, S.C.L. Koh, A. Acquaye, D. C. Sinclair, C. A. Randall, F. H. Abubakar, L. Smith, G. Schileo, and L. Ozawa-Meida, *J. Eur. Ceram. Soc.*, **38**, 4922 (2018).
doi: https://doi.org/10.1016/j.jeurceramsoc.2018.06.044

[16] S. Gao, *Semicond. Sci. Inf. Devices*, **1**, 14 (2019).
doi: https://doi.org/10.30564/ssid.v1i1.1171

[17] J. Yan and Y. G. Jeong, *ACS Appl. Mater. Interfaces*, **8**, 15700 (2016).
doi: https://doi.org/10.1021/acsami.6b02177

[18] M. H. Malakooti, F. Julé, and H. A. Sodano, *ACS Appl. Mater. Interfaces*, **10**, 38359 (2018).
doi: https://doi.org/10.1021/acsami.8b13643

[19] G. Zhang, Q. Liao, Z. Zhang, Q. Liang, Y. Zhao, X. Zheng, and Y. Zhang, *Adv. Sci.*, **3**, 1500257 (2016).
doi: https://doi.org/10.1002/advs.201500257

[20] S. H. Shin, Y. H. Kim, M. H. Lee, J. Y. Jung, and J. Nah, *ACS Nano*, **8**, 2766 (2014).
doi: https://doi.org/10.1021/nn406481k

[21] N. R. Alluri, A. Chandrasekhar, V. Vivekananthan, Y. Purusothaman, S. Selvarajan, J. H. Jeong, and S. J. Kim, *ACS Sustainable Chem. Eng.*, **5**, 4730 (2017).
doi: https://doi.org/10.1021/acssuschemeng.7b00117

[22] Y. Zhao, Q. Liao, G. Zhang, Z. Zhang, Q. Liang, X. Liao, and Y. Zhang, *Nano Energy*, **11**, 719 (2015).
doi: https://doi.org/10.1016/j.nanoen.2014.11.061

[23] J. Wu, N. Qin, and D. Bao, *Nano Energy*, **45**, 44 (2018).
doi: https://doi.org/10.1016/j.nanoen.2017.12.034

[24] Q. Tang, J. Wu, D. Kim, C. Franco, A. Terzopoulou, A. Veciana, J. Puigmartí-Luis, X. Z. Chen, B. J. Nelson, and S. Pané, *Adv. Funct. Mater.*, **32**, 2202180 (2022).
doi: https://doi.org/10.1002/adfm.202202180

[25] C. K. Jeong, C. Baek, A. I. Kingon, K. I. Park, and S. H. Kim, *Small*, **14**, 1704022 (2018).
doi: https://doi.org/10.1002/smll.201704022

[26] B. Jiang, J. Iocozzia, L. Zhao, H. Zhang, Y. W. Harn, Y. Chen, and Z. Lin, *Chem. Soc. Rev.*, **48**, 1194 (2019).
doi: https://doi.org/10.1039/C8CS00583D

[27] B. Zhao, L. Lin, and D. He, *J. Mater. Chem. A*, **1**, 1659 (2013).
doi: https://doi.org/10.1039/C2TA00755J

[28] J. He, P. Zhang, X. Liu, S. Wu, L. Hu, and L. Xu, *J. Mater. Sci.*, **51**, 7049 (2016).
doi: https://doi.org/10.1007/s10853-016-0005-6

[29] J. Yang, M. N. Saqib, F. Liu, and F. Zhong, *Food Hydrocolloids*, **141**, 108676 (2023).
doi: https://doi.org/10.1016/j.foodhyd.2023.108676

[30] J. X. Chen, J. W. Li, C. C. Cheng, and C. W. Chiu, *ACS Omega*, **7**, 793 (2022).
doi: https://doi.org/10.1021/acsomega.1c05451

[31] Y. Kim, P. Huh, and S. I. Yoo, *Macromol. Chem. Phys.*, **224**, 2200383 (2023).
doi: https://doi.org/10.1002/macp.202200383

[32] K. Y. Chun, S. Seo, and C. S. Han, *Adv. Mater.*, **34**, 2110082 (2022).
doi: https://doi.org/10.1002/adma.202110082

[33] Z. Yi, J. Huang, Z. Liu, J. Liu, and B. Yang, *IEEE Electron Device Lett.*, **41**, 183 (2020).
doi: https://doi.org/10.1109/LED.2019.295487